

Rapid muon tomography for border security

Anzori Sh. Georgadze¹

Institute for Nuclear Research, National Academy of Sciences of Ukraine, Prospekt Nauky 47, 03680 Kyiv, Ukraine

(*Electronic mail: a.sh.georgadze@gmail.com)

Cosmic-ray muon tomography is a promising technique for border security applications, leveraging highly penetrating cosmic-ray muons and their interactions with various materials to generate 3D images of large and dense objects, such as shipping containers. Using scattering and absorption of muons as they pass through dense cargo materials, muon tomography provides a viable solution for customs and border security by enabling the verification of shipping container declarations and preventing illegal trafficking. In this study, we utilized Monte Carlo simulations to evaluate the effectiveness of muon tomography for cargo characterization and contraband detection in various smuggling scenarios. Our results demonstrate that muon tomography can offer a novel approach to cargo inspection, moving beyond traditional 3D image reconstruction. Instead, it analyzes muon scattering and absorption rates in real time during scanning, enabling the prompt detection of discrepancies between actual cargo contents and declared goods within just 10 to 20 seconds. This method is particularly effective for cargo consisting of uniform loads composed of a single material or product, a common practice in shipping. Unlike traditional X-ray radiography, which analyzes detailed 2D images, muon tomography begins evaluating scatter-absorption rates within the first few seconds of scanning. This early assessment enables cargo evaluation long before a statistically reliable 3D image is formed, significantly improving scanning throughput without disrupting trade flow.

I. INTRODUCTION

Muon tomography is an emerging technique with promising applications in various fields such as non-destructive testing, underground cavities, archaeology, glaciers¹⁻⁵.

As global trade continues to expand, the challenge of intercepting illicit smuggling activities at borders has become increasingly complex. Traditional cargo inspection methods often struggle to keep pace with sophisticated concealment techniques employed by smugglers. Muon tomography has been proposed as a tool for border security applications⁶⁻²³. This technology, recently proposed to cargo inspection, offers unique capabilities. It provides exceptional penetration for effectively screening even the densest materials and cargo, surpassing the capabilities of traditional X-ray systems. Additionally, muon tomography is non-hazardous to humans and requires no shielding, allowing scanning sealed cargo without opening containers. The European project, "Cosmic Ray Tomograph for Identification of Hazardous and Illegal Goods hidden in Trucks and Sea Containers" (Silent-Border)²⁴, focuses on the development and in-situ testing of a high-technology scanner designed for border guards, customs, and law enforcement authorities to inspect shipping containers at border control points.

In this paper, several Monte Carlo (MC) simulation studies were conducted to evaluate the muon tomography method and the algorithms used for image reconstruction in container transshipment security applications. Various configurations and smuggling scenarios were considered and simulated. The goal was to develop a quantitative method for the rapid assessment of the presence of illegal and hazardous materials concealed within legitimate goods, as well as to create noise reduction techniques for visualizing hidden objects. The statistical method is used to compare the combined analysis of muon scattering and absorption rates for different material configurations obtained from the scan data, enabling the creation of a

map for the rapid assessment of customs declarations.

II. MATERIALS AND METHODS

We use GEANT4²⁵ to model various muon tomography scenarios for border security applications. This enables realistic simulations of muon interactions with cargo materials and hidden items. When muons interact with matter, they scatter, and by measuring the angles and intensities of these scattered muons it is possible to create 3D images of the interior of objects or structures. The fraction of cosmic muons can be absorbed by the crossed materials. Muon absorption depends on the density and composition of the material.

Cosmic-ray muons are naturally occurring charged particles generated in extensive atmospheric showers when high-energy cosmic rays from space interact with the Earth's atmosphere. Their flux at sea level is approximately $1 \text{ cm}^{-2} \text{ min}^{-1}$, with an average energy of about 3 GeV.

A. The Muon Scattering Tomography Method

The scattering muon tomography technique calculates the deflection of muons from their straight trajectory because of multiple coulomb interactions, which in turn depend on cargo density and chemical composition. The angular distribution of scattered muon of momentum p is approximately Gaussian, with zero mean and standard deviation given by:

$$\sigma_\theta = \frac{13.6 \text{ MeV}}{\beta c p} \sqrt{\frac{L}{X_0} (1 + 0.038 \ln \frac{L}{X_0})} \quad (1)$$

where β is the ratio between velocity of muon V to velocity of light c , X_0 is the radiation length of the material, L is the length of the material traversed. X_0 is a material property and depends on the density of the material ρ , the atomic mass A

and the atomic number Z and can be expressed as²⁶:

$$X_0 = \frac{716.4 \text{ g/cm}^2}{\rho} \frac{A}{Z(Z+1) \ln(287/\sqrt{Z})} \quad (2)$$

B. The Muon Absorption Method

In the absorption tomography approach, the tracks of muons stopped in the cargo can be reconstructed using an algorithm similar to that described in the publication²⁷⁻²⁹. The absorption muon tomography technique calculates the fraction of muons that were stopped in cargo by linking upper and lower tracking detectors. It focuses on muons detected by the upper detectors but absorbed within the imaging volume before reaching the lower detectors. The algorithm tracks muon paths and counts voxel crossings. Reconstructed muon tracks determine the path length d_{ij} of each muon through voxel j . The stopping power S_j represents the muon's energy loss per unit distance in that voxel. The total absorption $N_{abs,i}$ along a muon's path is the sum of stopping powers across all traversed voxels:

$$N_{abs,i} = \sum_j d_{ij} S_j \quad (3)$$

Muons interacting with the contents of a shipping container can be significantly deflected or even stopped due to their long path lengths, often extending meters, as shown in Figure 1. The extent of muon scattering and absorption depends on the cargo's density, resulting in distinct deflection and absorption patterns for different materials. This variation provides a viable method for material identification within shipping containers.

C. Cargo Inspection Procedures.

The cargo inspection process may follows a two-stage approach. In the first stage, a cargo image is reconstructed within 10–20 seconds of scanning, followed by an combined analysis of the cargo's scattering and absorption rates. These

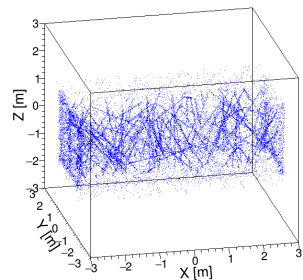


FIG. 1. Visualizations using GEANT4 of muon tracks ($n = 200$) in a shipping container with cargo, generated using the Cosmic Ray Shower Library (CRY)³⁰.

measured rates are then compared with the expected values predicted based on the customs declaration. If discrepancies are identified, the scanning process continues to create three-dimensional image ensuring statistically significant accuracy. Such a two-stage approach enhances the ability to validate inconsistencies and potentially visualize any concealed contraband within the cargo. Due to the different sizes and loading configurations of the cargo, in order to correctly verify cargo material object detection techniques have to be first applied to identify the shape and dimensions of the cargo in the reconstructed image of the container²³.

III. RESULTS

A. Modeling the Substitution of Declared Goods with Contraband.

We consider the substitution of declared clothes with high-value branded jeans. In this scenario, a portion of the declared low-cost cotton jeans is secretly replaced with high-end branded jeans to evade customs duties or import restrictions. This substitution can be detected in muon tomography because of differences in the packaging structure and material density.

In the GEANT4 simulation, the muon tomography station (MTS) is composed of plane detectors made of plastic scintillator, which have a 100% detection efficiency. The geometry of the MTS is illustrated in Figure 2(a). The MTS consists of tracking modules located at the top, bottom, and sides, with plane detector dimensions of $8 \times 4 \times 0.001 \text{ m}^3$, fully covering the shipping container. The GEANT4 model of a standard 20-foot shipping container (measuring $6.05 \times 2.59 \times 2.43 \text{ m}^3$) was filled with cargo on standard pallets, as shown in Figure 2(b). In this figure, bulk-packed cotton jeans are represented in yellow, while branded jeans in individual packaging, placed in boxes on pallets, are shown in cyan. Cheap cotton jeans were modeled as a textile made of cotton fiber with a bulk density of approximately 0.4 g/cm^3 , while branded jeans had a bulk density of about 0.2 g/cm^3 . The difference in bulk density arises from variations in packaging and air content rather than the chemical density of the fabric itself. Cheap jeans are typically packed in bulk, tightly compressed into

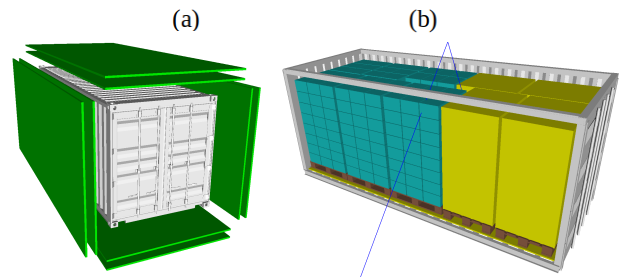


FIG. 2. (a) Schematic view of cosmic ray tomography station. (b) GEANT4 visualizations of a container with bulk-packed cotton jeans (yellow) and branded jeans (cyan) in individual packaging on pallets.

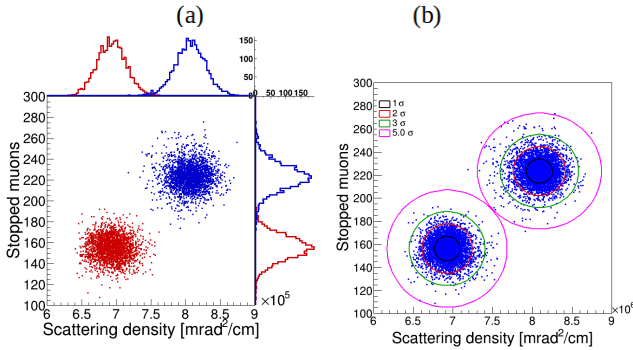


FIG. 3. (a) The distributions of 5,000 data samples generated for scenario of bulk-packed cotton jeans in container represented in blue, while scenario with partial substitution with branded jeans are shown in red. At the top of each 2D histogram, the corresponding 1D histograms for both distributions are displayed. (b) The same distributions are fitted with two component 2D Gaussian Mixture Model to quantify the discrimination accuracy between two scenarios. The black, red and green confidence ellipses for each distribution are set to show 1, 2 and 3 σ confidence levels (CL). The magenta confidence ellipses show the 5 σ CL at which the distributions are discriminated.

large cardboard boxes, minimizing air gaps and increasing bulk density. In contrast, branded jeans are often individually wrapped in plastic, placed in sturdier packaging, or folded differently, introducing more air pockets and resulting in a lower bulk density. Variations in cargo materials influence muon scattering and absorption rates, enabling the detection of discrepancies between uniform and substituted cargo sections. To verify the dependence of scatter-absorption rates on cargo material in this scenario, we simulated 5,000 data samples using the CRY muon generator with 100,000 muons sampled on a $10\text{ m} \times 10\text{ m}$ surface. This number of muons corresponds to approximately 10 seconds of scan time. At the top of each 2D histogram, the corresponding 1D histograms for both distributions are displayed. We apply the Point-of-Closest-Approach (PoCA) algorithm³¹ to determine the closest point between incoming and outgoing muon tracks and calculate the scattering angle.

To create images of cargo in this scenario we simulated 300,000 muons sampled on the surface $10\text{ m} \times 10\text{ m}$. This number of muons corresponds to approximately 30 seconds of scan time. As shown in the reconstructed images in Figure 4(a and b), the bright yellow color indicates regions of high scattering and absorption of muon tracks, corresponding to bulk-packed cotton jeans (with higher density), while the dark areas are attributed to low-density branded jeans in individual packaging (with lighter density). Processing image created using PoCA method is performed using ROOT package³². In this scenario, cargo substitution with contraband material can be detected within 10 seconds using statistical analysis of scatter-absorption rates and visualized within 30 seconds.

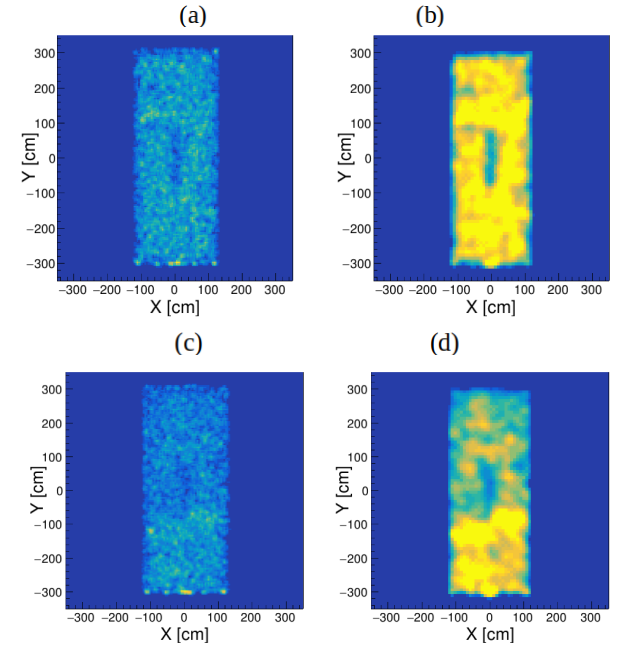


FIG. 4. Reconstructed XY projections of 3D PoCA images of a container filled with bulk-packed cotton jeans (a, b) and a container in which some of the pallets are replaced with individually packaged branded jeans (c, d). The simulated images were obtained by generating 300,000 muons using the CRY muon generator, corresponding to a scan time of 30 seconds. In (b) and (d), a threshold was applied during data processing to improve image contrast.

B. Modeling Hidden Hazardous Materials in Legal Cargo.

To simulate a scenario involving a shipping container loaded with cargo containing hidden hazardous materials, we used a GEANT4 model of a standard 20-foot shipping container (Figure 5a), containing legal cargo arranged in carton boxes placed on pallets. Among these boxes, hazardous materials are concealed. Specifically, one box on each pallet is loaded with explosive material—Royal Demolition eXplosive (RDX), which has a density of 1.812 g/cm^3 . To create a tomographic image of the shipping container, 5 million muons (equivalent to a 5-minute scanning time) were simulated using the CRY muon generator, sampled on a $10 \times 10\text{ m}^2$ surface. Figure 5b shows the 3D PoCA reconstruction after applying median filtering to reduce noise. In order to reject noise from legal cargo determine positions of hidden illegal goods and an estimate of their density besides image filtering we perform spatial cuts, removing PoCA points outside shipping container area. Next we subtract the image of an empty container from the 3D image of a loaded container.

To verify the applicability of rapid detection methods for the scenario of hidden RDX in cargo, we simulated 100,000 muons, sampled over a $10\text{ m} \times 10\text{ m}$ surface area, using the CRY generator. We considered two geometries: one where the container is loaded only with legal cargo (dry pasta, density 0.95 g/cm^3), and another where one box on each pallet is replaced with RDX. The 5 min scanning time images of con-

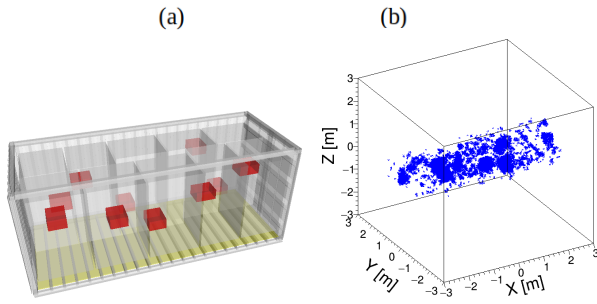


FIG. 5. (a) A GEANT4 simulation of a container where RDX is hidden within dry pasta placed on pallets. (b) Reconstructed 3D image of the container using the PoCA method. Median filtering is applied to the 3D reconstruction to reduce noise and improve visualization of hidden items.

tainer with explosive RDX hidden in 5 tones of cargo (clothes) are shown in figure 6. An advantage of muon tomography - segmentation of 3D image into slices makes possible detection of hidden explosive. Figures 6(a) and (b) shows results of statistical analysis demonstrating at which CL two scenarios are discriminated.

C. Simulation of Methamphetamine Concealment within Cement Shipments

Another important scenario for evaluating the performance of muon tomography involves the concealment of lower-density contraband materials within higher-density cargo. In such cases, the tomographic image reveals the illicit substance as localized regions of reduced scattering density, appearing as voids or anomalies, within the surrounding dense matrix. A representative real-world example of this scenario is the concealment of methamphetamine hydrochloride powder in-

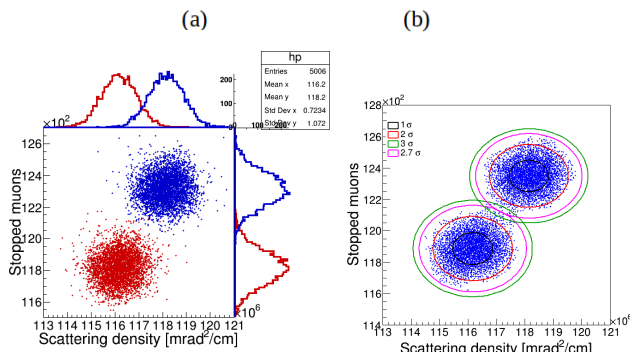


FIG. 6. (a) Histograms show the distribution of 5000 data samples for legal cargo - dry pasta (red data points) and the distribution of 5000 data samples for legal cargo mixed with 500 kg of RDX explosive randomly distributed in boxes on pallets (blue data points). (b) Scatter plots of data samples fitted to a two-component 2D Gaussian mixture model. The black, red and green confidence ellipses for each distribution are adjusted to show confidence levels (CL) of 1, 2 and 3 σ . The magenta confidence ellipses show CL 4.5 σ , at which the distributions are discriminated.

side cement bags⁷. Cement, being a high-density material, can effectively attenuate X-rays and is known to pose significant challenges for conventional radiographic screening techniques. This makes muon tomography particularly advantageous, as it relies on multiple scattering of naturally occurring cosmic muons rather than attenuation, thereby offering greater sensitivity to differences in atomic number (Z) and material density.

To simulate the concealment of methamphetamine, a volume of the drug was embedded within cement bags in a GEANT4-based geometry. The simplified scenario models a standard 20-foot shipping container loaded with six pallets of cement. Of these, four pallets contain concealed cubic packages of methamphetamine, each measuring $50 \times 50 \times 50$ cm³, hidden within the cement bags. The remaining two pallets consist solely of cement (see Figure 7(a)). Methamphetamine is an organic compound with the chemical formula C₁₀H₁₅N. In most smuggling cases, it is encountered as methamphetamine hydrochloride, with the formula C₁₀H₁₅N·HCl and an assumed density of 0.91 g/cm³⁷, reflecting the physical characteristics of methamphetamine hydrochloride powder commonly trafficked in illicit shipments. The surrounding material - cement was modeled with a bulk density of 1.4 g/cm³. Its chemical composition was approximated as follows: 61.66% CaO, 19.83% SiO₂, 2.32% Fe₂O₃, 4.48% Al₂O₃, 3.14% MgO, and 2.57% SO₃.

The 5,000,000 muons were simulated, corresponding to a scanning duration of 5 minutes. Figure 7(b) shows a reconstructed image using the PoCA method with subsequent filtering for noise reduction. Segmenting the tomographic image into slices is necessary to enable visualization of hidden lower-density contraband within higher-density cargo. Figure 8 displays the XY projections of two slices along the Z axis at different heights within the tomographic volume. In Figure 8(a), the upper slice crosses cement bags, which appear as regions with uniform distributions across all six palettes. In the lower slice (8(b)), the concealed methamphetamine, despite being embedded within dense cement, appears as a distinct region of lower scattering density due to its lower material density, making it clearly distinguishable from the surrounding cement bags.

D. Modeling high-Z special nuclear materials Hidden in Steel Pipes

Illicit trafficking of nuclear materials remains a critical security concern. We modeled a scenario where high-Z Special Nuclear Material (SNM) is concealed within steel pipes, common cargo items that can act as effective shielding. The GEANT4 model of container with pipes was created. We simulated one million muons sampled on the surface 10×10 cm² using CRY particle generator, which corresponds to a one-minute scan, to evaluate the system's detection capability. In this scenario, a shipping container is loaded with 166 steel pipes, each with a diameter of 16 cm, length of 500 cm and a thickness of 1 cm. Concealed within the pipes are three $10 \times 10 \times 10$ cm³ Special Nuclear Material (SNM) cubes (marked

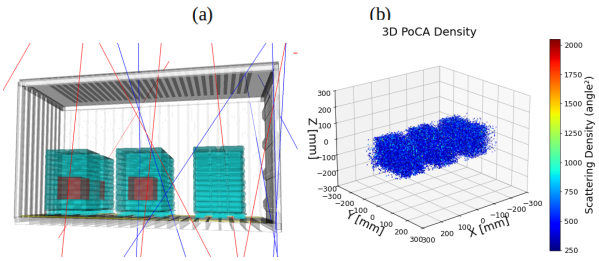


FIG. 7. (a) Conceptual illustration of the GEANT4 geometry representing the scenario in which methamphetamine is concealed within cement bags loaded on six pallets inside a 20-foot cargo container; (b) Simulated 3D tomographic reconstruction of concealed methamphetamine within the cement bags.

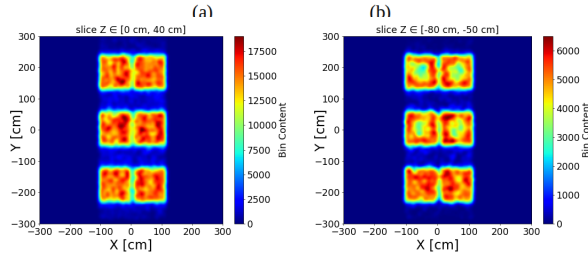


FIG. 8. (a) XY projection of the upper slice of the tomographic image, showing uniform distribution of cement bags across all pallets; (b) XY projection of a lower slice, revealing distinct lower scattering density regions corresponding to concealed methamphetamine within the cement cargo.

in red in Figure 9), strategically hidden within the dense steel structure to evade detection.

The simulated data were processed using PoCA imaging algorithm. Performing image processing an adaptive thresholding algorithm was employed to suppress noise originating from the surrounding steel structures. This significantly improved image clarity and reduced false positives. Subsequently, the DBSCAN clustering algorithm was applied to automatically identify and localize the three SNM objects within the reconstructed volume. Figure 10(a) presents the reconstructed 3D image processed using the DBSCAN algorithm. Three SNM cubes are detected and marked with different colors corresponding to the identified clusters. Figures 10(b)–(d) show the XY, YZ, and XZ 2D projections, respectively. These views provide a clearer visualization of the SNM cubes hid-

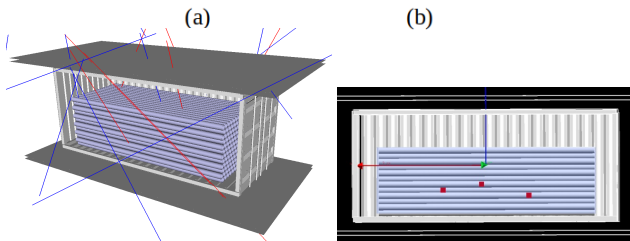


FIG. 9. A shipping container is loaded with steel pipes. Three 10 cm^3 cubes of SNM, represented in red, are concealed within the pipes.

den within the steel pipes. Noise from the surrounding steel structure has been effectively suppressed, enhancing both the image clarity and the detectability of SNM.

These results demonstrate the strong potential of real-time muon tomography combined with intelligent post-processing for the rapid detection of nuclear threats in dense and shielded cargo environments.

IV. DISCUSSION AND CONCLUSIONS

This study demonstrates the effectiveness of a two-stage cargo screening system based on muon tomography for real-time cargo composition estimation. The integration of scattering and absorption measurements offers a highly sensitive, non-invasive method for analyzing a wide range of cargo types, with strong potential for enhancing customs screening procedures.

The proposed approach involves a rapid initial scan (10–20 seconds) to evaluate scattering and absorption rates, followed by a second stage in which a 3D image is reconstructed within 1 to 5 minutes. Post-processing techniques are then applied to detect and localize concealed contraband materials with high precision.

Monte Carlo-simulated scenarios confirm the system's ability to rapidly detect discrepancies between declared cargo content and measured physical properties. Categories of detected contraband include:

- **Low-density, low-Z materials**, commonly used to disguise the misdeclaration of high-value goods.
- **Hazardous and volatile substances**, which pose immediate safety risks and require prompt identification.
- **Special Nuclear Materials (SNM)**, often deliberately shielded within dense cargo structures to evade conventional detection—posing a critical non-proliferation concern.

Advanced 3D image processing techniques, including median and Gaussian filtering and adaptive thresholding, significantly improve image clarity by suppressing structural noise and enhancing anomaly detection. These methods have proven effective in revealing both low-Z and high-Z concealed threats, even when embedded in complex or dense cargo configurations.

The highly sensitive data processing algorithms developed in this work establish muon tomography as a powerful complement to traditional X-ray imaging systems. Especially in cases involving shielded or irregular cargo where X-rays may fail, muon-based systems offer a robust, high-accuracy, and non-destructive solution for modern border security and cargo inspection.

Future work should focus on integrating machine learning for anomaly detection and expanding real-world testing to further validate performance under operational conditions.

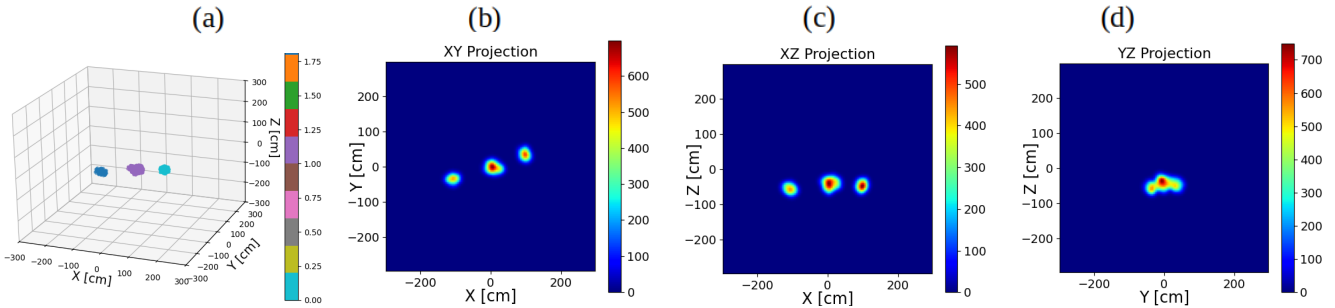


FIG. 10. (a) 3D visualization of three detected SNM cubes using the DBSCAN algorithm. The cubes are marked with different colors corresponding to the identified clusters. XY, YZ and XZ projections of tomographic image for 1 minute scanning time.

ACKNOWLEDGMENTS

This work was partially supported by the EU Horizon 2020 Research and Innovation Programme under grant agreement no. 101021812 (“SilentBorder”).

DATA AVAILABILITY STATEMENT

The data supporting this research are available from the corresponding author upon reasonable request.

V. REFERENCES

- ¹Hiroyuki KM Tanaka, Toshiyuki Nakano, Satoru Takahashi, Jyunya Yoshida, Minoru Takeo, Jun Oikawa, Takao Ohminato, Yosuke Aoki, Etsuro Koyama, Hiroshi Tsuji, et al. High resolution imaging in the inhomogeneous crust with cosmic-ray muon radiography: The density structure below the volcanic crater floor of mt. asama, japan. *Earth and Planetary Science Letters*, 263(1-2):104–113, 2007.
- ²Nolwenn Lesparre, Dominique Gibert, Jacques Marteau, Jean-Christophe Komorowski, Florence Nicollin, and Olivier Coutant. Density muon radiography of la soufrière of guadeloupe volcano: comparison with geological, electrical resistivity and gravity data. *Geophysical Journal International*, 190(2):1008–1019, 2012.
- ³Kunihiro Morishima, Mitsuaki Kuno, Akira Nishio, Nobuko Kitagawa, Yuta Manabe, Masaki Moto, Fumihiro Takasaki, Hirofumi Fujii, Kotaro Satoh, Hideyo Kodama, et al. Discovery of a big void in khufu’s pyramid by observation of cosmic-ray muons. *Nature*, 552(7685):386–390, 2017.
- ⁴Giulio Saracino, L Amato, Fabio Ambrosino, G Antonucci, Lorenzo Bonechi, Luigi Cimmino, Lucia Consiglio, RD’ Alessandro, E De Luzio, Ga Minin, et al. Imaging of underground cavities with cosmic-ray muons from observations at mt. etna (naples). *Scientific reports*, 7(1):1181, 2017.
- ⁵Ryuichi Nishiyama, Akitaka Ariga, T Ariga, Samuel Käser, A Lechmann, David Mair, Paola Scampoli, Mykhailo Vladymyrov, Antonio Ereditato, and F Schlunegger. First measurement of ice-bedrock interface of alpine glaciers by cosmic muon radiography. *Geophysical Research Letters*, 44(12):6244–6251, 2017.
- ⁶Larry Joe Schultz. *Cosmic ray muon radiography*. Portland State University, 2003.
- ⁷Lorenzo Bonechi, Raffaello D’Alessandro, and Andrea Giannanco. Atmospheric muons as an imaging tool. *Reviews in Physics*, 5:100038, 2020.
- ⁸Sarah Barnes et al. Cosmic-ray tomography for border security. *Instruments*, 7(1):13, 2023.
- ⁹K. N. Borozdin et al. Radiographic imaging with cosmic-ray muons. *Nature*, 422:277–277, 2003.
- ¹⁰L. Cuéllar et al. Soft cosmic ray tomography for detection of explosives. In *2009 IEEE Nuclear Science Symposium Conference Record (NSS/MIC)*, pages 968–970, 2009.
- ¹¹Zheng Yifan, Zeng Zhi, Zeng Ming, Wang Xuewu, and Zhao Ziran. Discrimination of drugs and explosives in cargo inspections by applying machine learning in muon tomography. *High Power Laser and Particle Beams*, 30(8):086002–1, 2018.
- ¹²E. Åström, G. Bonomi, I. Calliari, et al. Precision measurements of linear scattering density using muon tomography. *Journal of Instrumentation*, 11(07):P07010, jul 2016.
- ¹³P. Checchia. Review of possible applications of cosmic muon tomography. *Journal of Instrumentation*, 11(12):C12072, dec 2016.
- ¹⁴V. Antonuccio, M. Bandieramonte, U. Becciani, et al. The muon portal project: Design and construction of a scanning portal based on muon tomography. *Nuclear Instruments and Methods in Physics Research Section A: Accelerators, Spectrometers, Detectors and Associated Equipment*, 845:322–325, 2017. Proceedings of the Vienna Conference on Instrumentation 2016.
- ¹⁵C Pugliatti, V Antonuccio, M Bandieramonte, et al. Design of a muonic tomographic detector to scan travelling containers. *Journal of Instrumentation*, 9(05):C05029, may 2014.
- ¹⁶CL Morris, Jeffrey Bacon, Konstantin Borozdin, et al. A new method for imaging nuclear threats using cosmic ray muons. *AIP Advances*, 3(8), 2013.
- ¹⁷E Preziosi, F Arcieri, A Caltabiano, et al. Tecnomuse: a novel, rpc-based, muon tomography scanner for the control of container terminals. *Journal of Physics: Conference Series*, 1548(1):012021, may 2020.
- ¹⁸Jiahui Chen et al. Towards a muon scattering tomography system for both low-Z and high-Z materials. *Journal of Instrumentation*, 18(08):P08008, aug 2023.
- ¹⁹Anzori Sh. Georgadze and Vitaly A. Kudryavtsev. Geant4 simulation study of low-Z material detection using muon tomography. *Journal of Instrumentation*, 18(12):C12014, dec 2023.
- ²⁰Anzori Georgadze, Andrea Giannanco, Vitaly Kudryavtsev, Maxime Lagrange, and Cenk Turkoglu. A simulation of a cosmic ray tomography scanner for trucks and shipping containers. *Journal of Advanced Instrumentation in Science*, 2024(1), Mar. 2024.
- ²¹Anzori Sh Georgadze. Simulation study into the detection of low- and high-Z materials in cargo containers using cosmic ray muons. *Acta Physica Polonica B Proceedings Supplement*, 17(1):1–A2.1–1–A2.8, 2024.
- ²²Anzori Sh Georgadze. Rapid cargo verification with cosmic ray muon scattering and absorption tomography. *Journal of Instrumentation*, 19(07):P10033, 2024.
- ²³Anzori Sh Georgadze. Automated object detection for muon tomography data analysis. *Journal of Instrumentation*, 19(07):C07004, 2024.
- ²⁴European Commission. Cosmic ray tomograph for identification of hazardous and illegal goods hidden in trucks and sea containers. <https://doi.org/10.3030/101021812>.
- ²⁵S. Agostinelli, J. Allison, K. Amako, et al. Geant4—a simulation toolkit. *Nuclear Instruments and Methods in Physics Research Section A: Accelerators, Spectrometers, Detectors and Associated Equipment*, 506(3):250–303, 2003.

²⁶Gerald R. Lynch and Orin I. Dahl. Approximations to multiple coulomb scattering. *Nuclear Instruments and Methods in Physics Research Section B: Beam Interactions with Materials and Atoms*, 58(1):6–10, 1991.

²⁷S Vanini, P Calvini, P Checchia, A Rigoni Garola, J Klinger, G Zumerle, G Bonomi, A Donzella, and A Zenoni. Muography of different structures using muon scattering and absorption algorithms. *Philosophical Transactions of the Royal Society A*, 377(2137):20180051, 2019.

²⁸Gary Blanpied, Sankaran Kumar, Dustin Dorroh, Craig Morgan, Isabelle Blanpied, Michael Sossong, Shawn McKenney, and Beth Nelson. Material discrimination using scattering and stopping of cosmic ray muons and electrons: Differentiating heavier from lighter metals as well as low-atomic weight materials. *Nuclear Instruments and Methods in Physics Research Section A: Accelerators, Spectrometers, Detectors and Associated Equipment*, 784:352–358, 2015.

²⁹JA Rengifo and JL Bazo. Design of an atmospheric muon tomographer for material identification based on CORSIKA+GEANT4 simulations. *arXiv preprint arXiv:2403.14948*, 2024.

³⁰Chris Hagmann, David Lange, and Douglas Wright. Cosmic-ray shower generator (CRY) for monte carlo transport codes. In *2007 IEEE Nuclear Science Symposium Conference Record*, volume 2, pages 1143–1146, 2007.

³¹Richard Hoch, Debasis Mitra, Kondo Gnanvo, and Marcus Hohlmann. Muon tomography algorithms for nuclear threat detection. *Opportunities and challenges for next-generation applied intelligence*, pages 225–231, 2009.

³²Rene Brun and Fons Rademakers. Root — an object oriented data analysis framework. *Nuclear Instruments and Methods in Physics Research Section A: Accelerators, Spectrometers, Detectors and Associated Equipment*, 389(1):81–86, 1997. New Computing Techniques in Physics Research V.